Applied Physics Letters ARTICLE scitation.org/journal/apl

Partially coherent perfect vortex beam generated by an axicon phase

Cite as: Appl. Phys. Lett. **119**, 171108 (2021); doi: 10.1063/5.0071705
Submitted: 16 September 2021 · Accepted: 13 October 2021 ·
Published Online: 27 October 2021

Xiaofei Li,[1] Huazhe Wei,[1] Taco D. Visser,[1,2,3,a)] Yangjian Cai,[1,4,a)] and Xianlong Liu[1,a)]

AFFILIATIONS

[1]Shandong Provincial Engineering and Technical Center of Light Manipulation and Shandong Provincial Key Laboratory of Optics and Photonic Devices, School of Physics and Electronics, Shandong Normal University, Jinan 250014, China
[2]Department of Physics and Astronomy, Vrije Universiteit, Amsterdam, The Netherlands
[3]The Institute of Optics, University of Rochester, Rochester, New York 14627, USA
[4]School of Physical Science and Technology, Soochow University, Suzhou 215006, China

[a)]Authors to whom correspondence should be addressed: t.d.visser@vu.nl; yangjiancai@suda.edu.cn; and xianlongliu@sdnu.edu.cn

ABSTRACT

Vortex beams are structured light fields with a helical phase of the form $\exp(il\phi)$ that carries an optical angular momentum (OAM) of $l\hbar$ per photon. Such beams typically have a ring-shaped intensity with a radius that varies with l. Perfect vortex (PV) beams are designed to have a radius that is approximately uniform over a certain OAM range. Here, we report how spatial coherence can be used to maintain a fixed ring shape over a larger propagation distance and for a greater OAM range than is possible for fully coherent vortex beams. Our work is relevant for the application of PV beams in areas such as trapping, tweezing, and optical communications.

Over the last few decades, optical vortex (OV) beams[1,2] have shown their usefulness in many fields,[3] such as super-resolution imaging,[4] optical trapping,[5–7] optical communications,[8–13] and nanotechnology.[14] The phase term $\exp(il\phi)$, with l being the topological charge (TC), causes the wavefront to be helical. Furthermore, each photon carries an amount of OAM of $l\hbar$. OV beams typically have an on-axis zero of intensity surrounded by a ring of light whose radius scales with charge l.[1] In many applications, such as optical trapping, fiber-based communications, and radio frequency and microwave communication systems,[15–18] it is desirable to have an OAM beam whose radius is independent of the TC. Perfect vortex (PV) beams are designed to overcome this problem[19] and have been widely applied.[20–26] They can be generated by the Fourier transformation of a Bessel–Gauss beam.[27] Alternative methods are detailed in Refs. 28–34. A discussion of the actual "perfection" of PVBs is presented in Ref. 35 in which it was shown that the ring radius can only be made constant for a finite range of OAM values. Typically, the ring structure is only maintained over a limited distance from the focal plane in which the beam is produced. Increasing this distance while simultaneously making the ring radius less dependent on the TC is desirable for the applications described in Refs. 24–26. For all such applications, it is necessary to develop a simple and effective method to generate PV beams that not only approach the ideal independence of their intensity radius of the topological charge, but also maintain it over a longer propagation distance than thus far reported.

The spatial coherence of a light beam[36] determines how it propagates and scatters.[37] Manipulating the state of coherence, therefore, adds an additional degree of freedom in designing optical beams.[38] Here, we report how a partially coherent perfect vortex (PCPV) beam can be generated. We show that such beams maintain their ring structure over a larger distance than their fully coherent counterparts.

We began by considering how to create a desired structured light field. Such a field can be generated through a Fourier transform by introducing a desired modulation phase $\psi(\boldsymbol{\rho})$ into the input field. As described in Ref. 39, an axicon phase $-k\rho_0\boldsymbol{\rho}/f$ is imprinted onto a Gaussian vortex beam and then a PV beam can be generated in the focal plane after passing through a lens. Here, ρ_0 controls the ring radius, f denotes the focal length, and $k = 2\pi/\lambda$ is the wavenumber associated with the wavelength λ.

Let us consider a partially coherent scalar beam propagating along the z axis. In the space-frequency domain, its statistical properties in the cross section z may be characterized by the cross-spectral density (CSD) function, defined as

$$W_{\mathrm{in}}(\boldsymbol{\rho}_1, \boldsymbol{\rho}_2, \omega) = \langle U^*(\boldsymbol{\rho}_1, \omega) U(\boldsymbol{\rho}_2, \omega)\rangle. \tag{1}$$

Here, $U(\boldsymbol{\rho}, \omega)$ is the scalar field at a transverse position $\boldsymbol{\rho}$ at frequency ω, and the angular brackets indicate an ensemble average. From now on, we will omit the frequency dependence in our notation.

From the Collins formula for propagation through an astigmatic ABCD system,[40]

$$U_{\rm out}(\boldsymbol{\rho}_1') = -\frac{ik}{2\pi B}e^{ikL_0}\int d^2\rho_1 U(\boldsymbol{\rho}_1) \times \exp\left[\frac{ik}{2B}\left(A\rho_1^2 - 2\boldsymbol{\rho}_1\cdot\boldsymbol{\rho}_1' + D\rho_1'^2\right)\right], \quad (2)$$

it follows that the propagated CSD function for a field with an axicon phase $\psi(\boldsymbol{\rho}) = -k\rho_0\boldsymbol{\rho}/f$ equals

$$W_{\rm out}(\boldsymbol{\rho}_1',\boldsymbol{\rho}_2') = \left(\frac{k}{2\pi B}\right)^2 \exp\left\{-\frac{ik}{2B}\left[D\left(\boldsymbol{\rho}_1'^2 - \boldsymbol{\rho}_2'^2\right)\right]\right\} \times \int_{-\infty}^{\infty}\int_{-\infty}^{\infty} W_{\rm in}(\boldsymbol{\rho}_1,\boldsymbol{\rho}_2)\exp\left[i\psi(\boldsymbol{\rho}_1)\right]\exp\left[-i\psi(\boldsymbol{\rho}_2)\right] \times \exp\left\{-\frac{ik}{2B}\left[A\left(\boldsymbol{\rho}_1^2 - \boldsymbol{\rho}_2^2\right) - 2\left(\boldsymbol{\rho}_1\cdot\boldsymbol{\rho}_1' - \boldsymbol{\rho}_2\cdot\boldsymbol{\rho}_2'\right)\right]\right\} \times d^2\boldsymbol{\rho}_1 d^2\boldsymbol{\rho}_2, \quad (3)$$

where $\boldsymbol{\rho} = (\rho,\phi)$, $\boldsymbol{\rho}' = (\rho',\phi')$ denotes the position vector in cylindrical coordinates. To characterize PCPV beams, we explore two cases. The first case we consider is propagation from the front focal plane of a lens to its back focal plane for generating such a beam [see Fig. 1(a)]. The ABCD transfer matrix is then

$$\begin{pmatrix} A_1 & B_1 \\ C_1 & D_1 \end{pmatrix} = \begin{pmatrix} 1 & f_1 \\ 0 & 1 \end{pmatrix}\begin{pmatrix} 1 & 0 \\ -1/f_1 & 1 \end{pmatrix}\begin{pmatrix} 1 & f_1 \\ 0 & 1 \end{pmatrix} = \begin{pmatrix} 0 & f_1 \\ -1/f_1 & 0 \end{pmatrix}, \quad (4)$$

where f_1 denotes the focal length. The second case is the previous process followed by a lens (with focal length f_2) and propagation over a distance z [see Fig. 1(b)]. We then have

$$\begin{pmatrix} A_2 & B_2 \\ C_2 & D_2 \end{pmatrix} = \begin{pmatrix} 1 & z \\ 0 & 1 \end{pmatrix}\begin{pmatrix} 1 & 0 \\ -1/f_2 & 1 \end{pmatrix}\begin{pmatrix} A_1 & B_1 \\ C_1 & D_1 \end{pmatrix} = \begin{pmatrix} -z/f_1 & f_1 - zf_1/f_2 \\ -1/f_1 & -f_1/f_2 \end{pmatrix}. \quad (5)$$

Here, the Gaussian–Schell model vortex (GSMV) beam is the input beam, and its CSD function reads[41]

$$W_{\rm in}(\rho_1,\phi_1,\rho_2,\phi_2) = \langle U^*(\boldsymbol{\rho}_1)U(\boldsymbol{\rho}_2)\rangle = \exp\left(-\frac{\rho_1^2+\rho_2^2}{w^2}\right)\exp\left[-\frac{\rho_1^2+\rho_2^2-2\rho_1\rho_2\cos(\phi_1-\phi_2)}{2\sigma_c^2}\right] \times \exp\left[il(\phi_1-\phi_2)\right], \quad (6)$$

where w and σ_c are the beam waist radius and the coherence radius, respectively. Furthermore, l represents the TC.

Applying Eqs. (3), (4), and (6), the intensity $I(\rho,\phi)$ in the back focal plane can be calculated. In Fig. 2, we display the intensity profile of a PCPV beam with $w = 0.68$ mm, $\rho_0 = 5w$, and $\sigma_c = 1$, 0.45, and 0.15 mm for different TCs. It is seen that the ring radius is independent of the topological charge l, and the ring thickness slightly increases when the coherence radius σ_c decreases. By comparing different rows, it can be seen that the beam with different TCs has the same ring radius. By comparing the first three columns that represent different coherence radii, it is shown that the coherence radius has a special effect on the ring. The width of the ring is somewhat larger when σ_c has a lower value. In contrast to the random beam, which does not have a definite phase, its CSD function does have a well-defined phase. This phase can be used to determine the beam's TC. We use the reference point $\boldsymbol{\rho}_2' = 0$, in which case the CSD function $W_{\rm out}(\boldsymbol{\rho}_1',\boldsymbol{\rho}_2')$ simplifies to $W_{\rm out}(\boldsymbol{\rho}_1',0)$. This is shown in the right-most column of Fig. 2 for the case $\sigma_c = 0.15$ mm. From top to bottom, there are 0, 2, and 5 phase singularities. These numbers correspond exactly to the TC. Moreover, the sign of the TC can be determined from the direction of these screw dislocations with a clockwise (counterclockwise) corresponding to a positive (negative) TC.

Further simulations are presented in Fig. 3. In panel (a), it is seen that the position of the peak intensity does not change with l, but that of the ring gradually broadens for larger values of the topological charge. In panel (b), one sees that when the coherence radius is decreased, the ring width gets somewhat larger [see Fig. 3(b)].

To further explore the properties of PCPV beams, by applying Eqs. (3), (5), and (6), we examine the propagation evolution of beams with different coherence radii when $l = 5$. This is shown in Fig. 4. When the beam is relatively spatially coherent, with $\sigma_c = 1$ mm, the

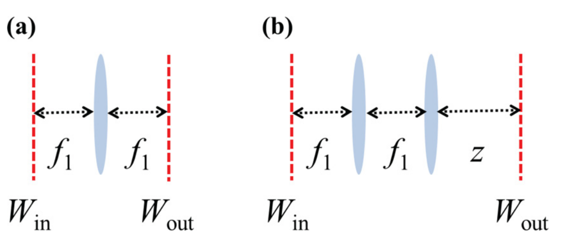

FIG. 1. Schematic representation of the generation of a partially coherent perfect vortex beam (a) and its propagation (b).

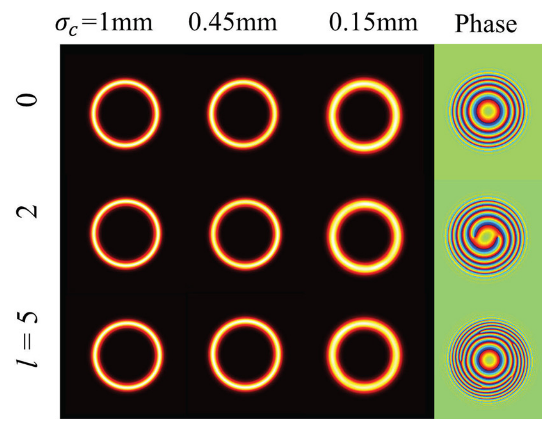

FIG. 2. Simulation of the intensity profile and the CSD phase of PCPV beams with different topological charges and coherence radii.

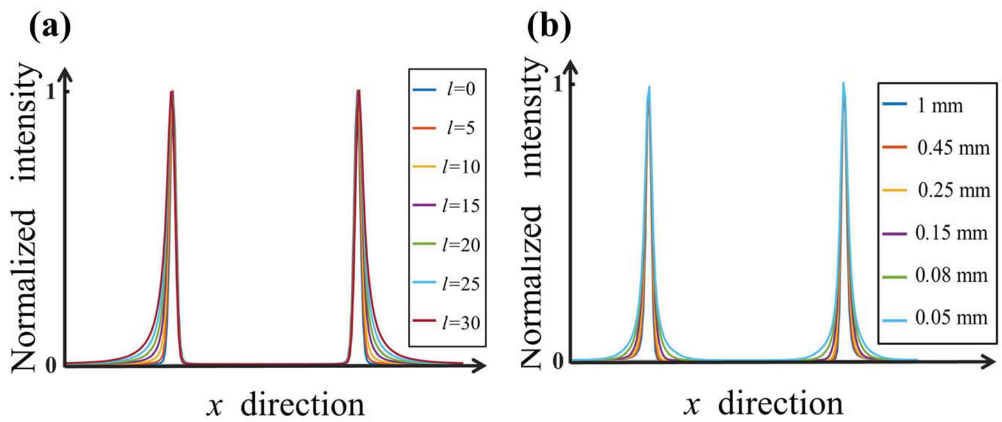

FIG. 3. (a) Cross section of the intensity of beams with different topological charges with $\sigma_c = 0.15$ mm. (b) Cross section of the intensity for different coherence radii when $l = 5$.

intensity profile develops unwanted secondary rings on propagation. When the spatial coherence radius decreases, this effect is seen to disappear. This indicates that the spatial coherence is a tool to create PCPV beams that are more robust on propagation. For a coherence radius of $\sigma_c = 0.25$ mm, the beam remains "perfect" up $z = 0.7f$ and the unwanted secondary rings gradually appear at $z = 0.8f$. Moreover, the ring structure can be maintained even over a distance $z = 0.8f$, when σ_c is lowered to 0.15 mm. This means that degradation of the ring structure can be alleviated by modulating the degree of coherence. The intensity ring can stay intact almost to $z = f$ when the coherence radius is small enough.

The physical mechanism behind our results lies in the role that the spatial coherence plays in interference. The spatial coherence of narrowband fields determines their capability to form sharp intensity patterns. As the coherence radius σ_c decreases, the intensity profile in any cross sections of the beam becomes slightly more diffuse. This is seen in the third column of Fig. 2, where the ring-shaped intensity is somewhat broader than in the first two columns that correspond to more coherent fields. A similar effect is observed in Fig. 4. The propagated beam corresponding to $\sigma_c = 0.15$ mm has an intensity profile that is just as broad as its more coherent counterparts, but it does not exhibit the unwanted secondary rings.

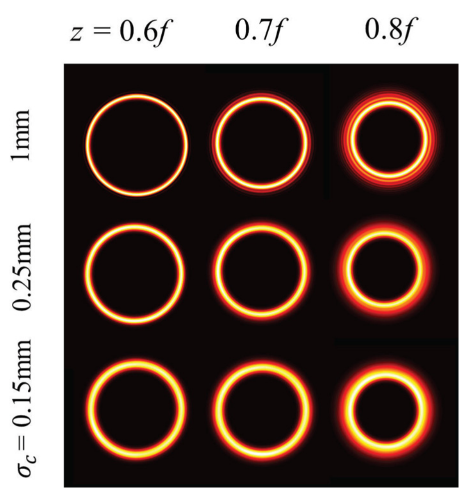

FIG. 4. Simulation of the normalized intensity evolution of the PCPV beam ($l = 5$) with different coherence radii for different propagation distances.

To prove the feasibility of our approach, we carried out the experiment sketched in Fig. 5. The output of a continuous-wave-diode-pumped laser operating at $\lambda = 532$ nm is passed through a neutral density filter and focused by L_1 ($f = 150$ mm) onto a rotating ground glass disk. The coherence radius σ_c can be modulated by changing the distance between the lens L_1 and the rotating ground glass disk.[42] After the collimating lens L_2 ($f = 150$ mm) and the Gaussian amplitude filter, the field is reflected off a spatial light modulator (SLM). This imprints both a phase hologram and the axicon phase onto the beam. The SLM is located in the front focal plane of the Fourier transform lens L_3 ($f = 400$ mm). After this lens, the beam is divided into two parts by a beam splitter. Part 1 and part 2 are for studying the generated ring structure and its propagation, respectively.

Figure 6 shows the intensity that is recorded by CCD_1, which is located in the back focal plane of L_3, for beams with different topological charge l and selected values of the coherence radius σ_c. It is verified

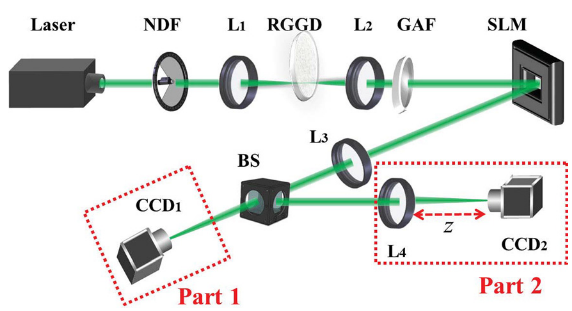

FIG. 5. Setup for the generation, propagation, and focusing of a PCPV beam. NDF: neutral density filter; L: thin lens; RGGD: rotating ground glass disk; GAF: Gaussian amplitude filter; SLM: spatial light modulator; BS: beam splitter; and CCD: charge coupled device.

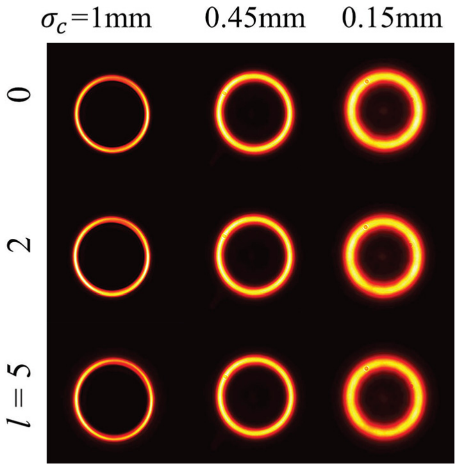

FIG. 6. Experimental results of the intensity profile of PCPV beams with different topological charges and coherence radii.

that the intensity radius of the beam does not vary with the topological charge. Also, the width of the intensity ring can be tuned by varying σ_c. The measurements are in good agreement with the simulation results shown in Fig. 2.

In Fig. 7, the lens L_4 with focal length ($f = 150$ mm) is located in the back focal plane of L_3. The intensity profile of the PCPV beams, as measured with CCD_2, is plotted for various propagation distances. Again the agreement with simulation in Fig. 4 is quite good. It is seen that decreasing the spatial coherence radius results in a beam, which maintains the structure of its intensity ring over a longer distance than its fully coherent counterpart.

In summary, we proposed a method for the generation of PCPV beams and investigated their properties experimentally. Our results clearly show that such beams can be generated by imprinting a GSMV beam with an axicon phase. The beam radius is shown to be constant when the topological charge is varied over a wide interval. The thickness of the intensity ring can be varied by changing the coherence radius. Moreover, partially coherent PV beams remain intact over a longer propagation distance than their spatially fully coherent counterparts. Our work extends the category of PV beams and may find applications in optical trapping and fiber-based technologies.

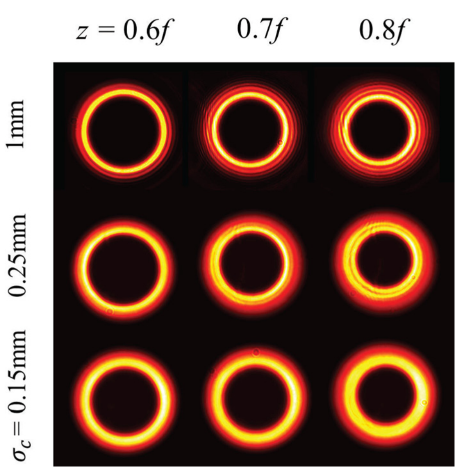

FIG. 7. Experimental results of the normalized intensity evolution of a PCPV beam ($l = 5$) with different coherence radii for different propagation distances as measured from lens L_4.

This work was supported by the National Key Research and Development Program of China (Grant No. 2019YFA0705000); the National Natural Science Foundation of China (Grant Nos. 11804198, 91750201, 11525418, and 11974218); the Shandong Provincial Natural Science Foundation of China (Grant No. ZR2019BA030); the Innovation Group of Jinan (Grant No. 2018GXRC010); the Local Science and Technology Development Project of the Central Government (Grant No. YDZX20203700001766); and the China Postdoctoral Science Foundation (Grant No. 2018M642690). T.D.V. acknowledges funding by The Dutch Research Council (NWO) under project P19–13 "Optical wireless super highways."

AUTHOR DECLARATIONS

Conflict of Interest

The authors declare that they have no conflicts of interest.

Author Contributions

All authors contributed equally to this work.

DATA AVAILABILITY

The data that support the findings of this study are available from the corresponding authors upon reasonable request.

REFERENCES

[1]L. Allen, M. W. Beijersbergen, R. J. C. Spreeuw, and J. P. Woerdman, Phys. Rev. A **45**, 8185 (1992).
[2]L. Allen, M. J. Padgett, and M. Babikera, Prog. Opt. **39**, 291 (1999).
[3]Y. Shen, X. Wang, Z. Xie, C. Min, X. Fu, Q. Liu, M. Gong, and X. Yuan, Light: Sci. Appl. **8**, 90 (2019).
[4]K. Liu, Y. Cheng, Y. Gao, X. Li, Y. Qin, and H. Wang, Appl. Phys. Lett. **110**, 164102 (2017).
[5]Y. Li, N. Zhao, and L. Zhou, Opt. Lett. **46**, 106 (2021).
[6]X. Li, H. Ma, H. Zhang, M. Tang, H. Li, J. Tang, and Y. Wang, Appl. Phys. Lett. **114**, 081903 (2019).
[7]H. Zhang, X. Li, H. Ma, M. Tang, H. Li, J. Tang, and Y. Cai, Opt. Express **27**, 22930 (2019).
[8]Q. Zhao, P. Yu, Y. Liu, Z. Wang, Y. Li, and L. Gong, Appl. Phys. Lett. **116**, 181101 (2020).
[9]R. Zhang, L. Li, Z. Zhao, G. Xie, G. Milione, H. Song, P. Liao, C. Liu, H. Song, K. Pang, A. N. Willner, B. Lynn, R. Bock, M. Tur, and A. E. Willner, Opt. Lett. **44**, 691 (2019).
[10]S. Fu, Y. Zhai, H. Zhou, J. Zhang, T. Wang, C. Yin, and C. Gao, Opt. Lett. **44**, 4753 (2019).
[11]Y. Chen, W. Shen, Z. Li, C. Hu, Z. Yan, Z. Jiao, J. Gao, M. Cao, K. Sun, and X. Jin, PhotoniX **1**, 5 (2020).
[12]S. Fu, Y. Zhai, J. Zhang, X. Liu, R. Song, H. Zhou, and C. Gao, PhotoniX **1**, 19 (2020).
[13]Z. Qiao, Z. Wan, G. Xie, J. Wang, L. Qian, and D. Fan, PhotoniX **1**, 13 (2020).
[14]C. Qiu and Y. Yang, Science **357**, 645 (2017).
[15]B. Thidé, H. Then, J. Sjöholm, K. Palmer, J. Bergman, T. D. Carozzi, Y. N. Istomin, N. H. Ibragimov, and R. Khamitova, Phys. Rev. Lett. **99**, 087701 (2007).

[16]S. M. Mohammadi, L. K. S. Daldorff, J. E. S. Bergman, R. L. Karlsson, B. Thidé, K. Forozesh, T. D. Carozzi, and B. Isham, IEEE Trans. Antennas Propag. **58**, 565 (2010).
[17]F. Tamburini, E. Mari, B. Thidé, C. Barbieri, and F. Romanato, Appl. Phys. Lett. **99**, 204102 (2011).
[18]M. Barbuto, M. Miri, A. Alù, F. Bilotti, and A. Toscano, IEEE Trans. Antennas Propag. **68**, 1851 (2020).
[19]A. S. Ostrovsky, C. Rickenstorff-Parrao, and V. Arrizón, Opt. Lett. **38**, 534 (2013).
[20]N. A. Chaitanya, M. Jabir, and G. K. Samanta, Opt. Lett. **41**, 1348 (2016).
[21]C. Zhang, C. Min, L. Du, and X. C. Yuan, Appl. Phys. Lett. **108**, 201601 (2016).
[22]P. Li, Y. Zhang, S. Liu, C. Ma, L. Han, H. Cheng, and J. Zhao, Opt. Lett. **41**, 2205 (2016).
[23]X. Li, H. Ma, C. Yin, J. Tang, H. Li, M. Tang, J. Wang, Y. Tai, X. Li, and Y. Wang, Opt. Express **26**, 651 (2018).
[24]W. Shao, S. Huang, X. Liu, and M. Chen, Opt. Commun. **427**, 545 (2018).
[25]F. Zhu, S. Huang, W. Shao, J. Zhang, M. Chen, W. Zhang, and J. Zeng, Opt. Commun. **396**, 50 (2017).
[26]M. K. Karahroudi, S. A. Moosavi, A. Mobasheery, B. Parmoon, and H. Saghafifar, Appl. Opt. **57**, 9148 (2018).
[27]F. Gori, G. Guattari, and C. Padovani, Opt. Commun. **64**, 491 (1987).
[28]M. Chen, M. Mazilu, Y. Arita, E. M. Weight, and K. Dholakia, Opt. Lett. **38**, 4919 (2013).
[29]P. Vaity and L. Rusch, Opt. Lett. **40**, 597 (2015).
[30]A. A. Kovalev, V. V. Kotlyar, and A. P. Porfirev, Appl. Phys. Lett. **110**, 261102 (2017).
[31]D. Li, C. Chang, S. Nie, S. Feng, J. Ma, and C. Yuan, Appl. Phys. Lett. **113**, 121101 (2018).
[32]A. Porfirev and A. Kuchmizhak, Appl. Phys. Lett. **113**, 171105 (2018).
[33]Y. Liang, S. Yan, M. He, M. Li, Y. Cai, Z. Wang, M. Lei, and B. Yao, Opt. Lett. **44**, 1504 (2019).
[34]Z. Gu, D. Yin, S. Nie, S. Feng, F. Xing, J. Ma, and C. Yuan, Appl. Phys. Lett. **127**, 163103 (2020).
[35]J. Pinnell, V. R. Fajardo, and A. Forbes, Opt. Lett. **44**, 5614 (2019).
[36]L. Mandel and E. Wolf, *Optical Coherence and Quantum Optics* (Cambridge University, 1995).
[37]D. G. Fischer, T. van Dijk, T. D. Visser, and E. Wolf, J. Opt. Soc. Am. A **29**, 78 (2012).
[38]D. Peng, Z. Huang, Y. Liu, Y. Chen, F. Wang, S. A. Ponomarenko, and Y. Cai, PhotoniX **2**, 6 (2021).
[39]D. Deng, Y. Li, Y. Han, X. Su, J. Ye, J. Gao, Q. Sun, and S. Qu, Opt. Express **24**, 28270 (2016).
[40]A. E. Siegman, *Lasers* (University Science Books, 1986).
[41]Y. Cai, Y. Chen, and F. Wang, J. Opt. Soc. Am. A **31**, 2083 (2014).
[42]F. Wang, S. Zhu, and Y. Cai, Opt. Lett. **36**, 3281 (2011).